# Automated Stenosis Detection in Coronary Artery Disease Using YOLOv9c: Enhanced Efficiency and Accuracy in Real-Time Applications

**Muhammet AKGÜL**
Sağlık Bilimleri Üniversitesi
**Hasan İbrahim KOZAN**
Necmettin Erbakan University
**Hasan Ali AKYÜREK**
hsnakyurek@gmail.com
Necmettin Erbakan University
**Şakir TAŞDEMİR**
Selçuk University

**Research Article**

**Keywords:** Coronary artery disease, stenosis detection, YOLOv9, multivessel disease, CAD diagnosis, detection accuracy

**Posted Date:** August 27th, 2024

**DOI:** https://doi.org/10.21203/rs.3.rs-4774572/v1



**Additional Declarations:** No competing interests reported.

**Version of Record:** A version of this preprint was published at Journal of Real-Time Image Processing on September 27th, 2024. See the published version at https://doi.org/10.1007/s11554-024-01558-x.

# Abstract

Coronary artery disease (CAD) is a prevalent cardiovascular condition and a leading cause of mortality. An accurate and timely diagnosis of CAD is crucial for treatment. In this study, we aimed to develop a novel stenosis detection algorithm using the YOLOv9c model to automate the detection of CAD for real-time applications. The dataset consisted of angiographic imaging series obtained from 100 patients with confirmed one-vessel CAD, comprising a total of 8,325 grayscale images. The YOLOv9c model was trained, tested, and validated using the Python API for YOLO and the ultralytics library, with fine-tuning and augmentations applied to improve detection accuracy. By automating the detection of multivessel disease, the proposed algorithm has the potential to enhance the workflow of operators. The proposed YOLOv9c model demonstrated superior performance in processing speed and detection accuracy, achieving an F1-score of 0.98 and an mAP@0.5 of 0.98, outperforming established models. The model had a weight of 25.3M, significantly lower than others, leading to reduced training time (11 hrs), fine-tuning time (3.5 hrs) and inference time (18 ms). Additionally, compared with SSD MobileNet V1, F1-score and mAP@0.5 improved by 1.36x and 1.42x, respectively. The proposed stenosis detection algorithm represents a significant advancement in the field of cardiovascular imaging and diagnostic algorithms. The integration of advanced algorithms in cardiovascular imaging represents a critical aspect of optimizing diagnostic efficiency and accuracy, emphasizing the need for ongoing advancements in medical imaging research and technology.


# 1. Introduction

CAD is a prevalent and life-threatening cardiovascular condition recognized as the leading cause of mortality in both developed and developing countries [1]. It is characterized by atherosclerosis and inflammation and leads to various clinical manifestations, such as stable angina, unstable angina, myocardial infarction (MI), and sudden cardiac death [2]. The genetic underpinnings of CAD have been extensively studied through genome-wide association studies (GWASs), which have identified several robustly associated genetic variants linked to CAD susceptibility [3]. These findings underscore the complex interplay between genetic predisposition and environmental factors in the development of CAD, highlighting the need for comprehensive understanding and advanced diagnostic approaches to address this multifaceted disease [2, 4].

Furthermore, the pathogenesis of CAD involves intricate cellular and molecular mechanisms, including the reprogramming of venous cells for the formation of coronary arteries, as well as the role of microRNAs and genetic correlates in diverse ancestral populations [5–7]. Additionally, the identification of risk loci for CAD and MI, such as ADAMTS7 and the ABO blood group system, has provided valuable insights into the genetic basis of these conditions [8, 9]. The significance of coronary artery development and anomalies, as well as the role of matrix metalloproteinases and tissue inhibitors in CAD, further elucidate the multifaceted nature of this disease [10, 11].

Moreover, the economic burden of CAD is substantial, with direct and indirect costs posing a significant impact on healthcare systems and society [12]. The prevalence of asymptomatic CAD in patients with diabetes mellitus underscores the challenges in the early detection and management of this high-risk population [12]. Additionally, the identification of novel susceptibility loci and the role of breast arterial calcification as a predictor of CAD risk highlight the evolving landscape of CAD research and diagnostic paradigms [13, 14].

American health-care providers estimate that 71 million adults have at least 1 cardiovascular disease, which accounts for 12 million cases of CAD and 5 million cases of heart failure [15]. Furthermore, as a previous study indicated, CAD was the most popular diagnosis in emergency departments [16]. The direct and indirect costs of CAD are about to be $3000 per patient each year in the United States of America [17].

Coronary heart disease is the most common type of heart disease, killing 375,476 people in 2021. Approximately 1 in 20 adults aged > 20 years have CAD (approximately 5%) [18]. In 2021, approximately 2 in 10 deaths from CAD occurred in adults younger than 65 years [19]. It has also been reported that CAD is the principal cause of cardiovascular mortality worldwide [20]. CAD is a serious threat to societies, as it is the leading cause of death in most countries worldwide [21]. With 13% of the deaths being due to CAD, the 2010 Global Burden of Disease Study identified it as a modern pandemic [22].

Accurate and timely diagnosis plays a crucial role in improving outcomes for patients with CAD, a leading cause of mortality worldwide [23]. Current methodologies in cardiovascular imaging predominantly depend on qualitative visual evaluation and basic quantitative analyses of cardiac structure and function. To augment the diagnostic efficacy of cardiac imaging, there is an urgent requirement for sophisticated image analysis techniques that facilitate more exhaustive quantification of imaging phenotypes. [24]. By leveraging these advanced techniques, we can gain deeper insights into the pathophysiology of CAD and optimize diagnostic decision-making for better patient management and treatment outcomes.

Object detection (OD) is a fundamental task in computer vision involving the identification and localization of specific objects within images, videos, or real-time applications [25]. YOLO (You Only Look Once) has emerged as a popular technology for OD in various industrial applications, enabling real-time object detection by dividing input images into a grid and predicting bounding boxes and class probabilities for each grid cell [26]. This approach allows for efficient and rapid object detection, as it requires a single forward pass through the network [27]. In the context of cardiovascular diseases, several OD algorithms have been utilized for tasks such as vessel segmentation in X-ray coronary angiography and CAD detection using computer tomography images [28]. Notably, the YOLO algorithm has been employed for developing deep learning-based techniques for CAD detection, demonstrating its versatility and potential in medical imaging applications [29, 30].

Despite the widespread use of OD algorithms in cardiovascular imaging, there is a notable gap in the literature regarding the application of YOLOv9 for coronary artery stenosis detection [31]. A recent study

addressed this gap by leveraging the YOLOv9 algorithm to achieve a high-accuracy diagnosis of coronary artery stenosis, demonstrating its effectiveness in comparison to similar studies [32]. This highlights the potential of advanced OD technologies, such as YOLOv9, to enhance diagnostic capabilities for cardiovascular conditions, emphasizing the need for further exploration and integration of cutting-edge algorithms in medical imaging research [33, 34].

In the context of medical imaging, the application of advanced augmentation techniques, such as mosaic augmentation, has potential for enhancing the robustness and generalizability of object detection models in tasks such as coronary artery stenosis detection and analysis of cardiovascular imaging data [35]. The strategic adaptation of augmentation strategies in deep learning frameworks, including YOLOv9, reflects ongoing efforts to optimize training processes and improve the diagnostic capabilities of medical imaging technologies [14, 36].

YOLOv9 was more successful than the previous versions. As shown in Fig. 1, YOLOv9 had better $mAP^{50–95}$ values than did YOLOv8, YOLOv7, YOLOv6-3.0 and YOLOv5-7.0 for both parameters and FLOPs (Floating Point Operations per second, in billions) on A100 TensorRt FP16.

However, although several studies have been performed on coronary artery stenosis detection based on modern neural networks [38], no study has focused on object detection via YOLOv9. In this study, the object detection technology emphasized above was utilized to achieve high-accuracy diagnosis of coronary artery stenosis. Within this scope, the YOLO algorithm was chosen among the object detection algorithms, and it was found to have a high accuracy rate compared to similar studies.

## 2. Materials and Methods

# 2.1 Source data

The dataset used for the present study consisted of angiographic images from 100 patients who underwent coronary angiography performed using the CoroScope and Innova image-guided surgery systems [39]. The patients had confirmed one-vessel CAD. The dataset includes 8,325 grayscale images of stenotic coronary arteries labeled using LabelBox. The stenotic regions were categorized based on size [38].

# 2.2 Architecture

In the YOLOv9 architecture, The Generalized Efficient Layer Aggregation Network (GELAN) and Programmable Gradient Information (PGI) are combined to produce a novel design that greatly enhances gradient flow and information retention. By addressing the issues of gradient reliability and information bottleneck, this combination helps the model learn from complicated data patterns more precisely and effectively without sacrificing any information.

Programmable Gradient Information (PGI) includes three main components,1) main branch,2) auxiliary reversible branch, and 3) multi-level auxiliary information. The main branch doesn't have any updates, while others are used to solve the problems, auxiliary reversible branch is used to solve deeping of neural networks problems, auxiliary reversibly branch provides informations that moves from the target to the data [37].

Generalized ELAN (GELAN) is a new network architecture created by combining two neural network architectures, these architectures are CSPNet and ELAN [37].

## 2.3 Model training, testing, validation and principle

In this study, a novel Python API for YOLO was used and employed by the YOLO library to streamline the entire workflow within a Gradient Notebook environment. The training, testing, and validating phases were performed on a workstation with an I9-14900K CPU, 64 GB of RAM and a NVIDIA RTX A4000 GPU. The primary objective was to construct a YOLOv9c model from the ground up utilizing the preconfigured settings and weights provided. Subsequently, the model was fine-tuned using the recently loaded dataset, with the model.train() method being employed.

During the training process, YOLOv9 undergoes a series of augmentations, including mosaic augmentation, which involves combining four images to introduce variations and occlusions, thereby compelling the model to learn object identities in new contexts [40]. However, continuous application of mosaic augmentation throughout the entire training regime may have a detrimental effect on prediction accuracy. To address this, YOLOv9c was designed to terminate the mosaic augmentation process during the final epochs of training, allowing for an optimal training pattern without compromising the overall training performance [9, 41].

Figure 2 illustrates the general flow of principles underlying this study. The process begins with the acquisition of primary images to be used in the outcome, accompanied by annotations. All acquired images undergo image preprocessing to make them fully usable in subsequent processes. Following preprocessing, the obtained data are splitted into three parts for training, testing, and validation, as mentioned above. Subsequently, prior to the testing and prediction phase, a fine-tuning process is applied to transfer learning, where the parameters of a pre-trained model are retrained on new data. Finally, the detection of angiography images is tested, and predictions for angiography image outcomes are made.

# 3. Results

YOLOv9s, YOLOv9m and YOLOv9c were used for preliminary analysis, and YOLOv9c was selected for study. The size, $mAP^{val}$, speed (CPU ONNX), speed (A100 TensorRT (ms), params (millions), and FLOPS (billions) parameters are given in Table 1. The brief parameters used are given in Table 2.

Table 1
Model features of YOLOv9c

| Model | Size (px) | $mAP^{val}$ 50-95 | Speed CPU ONNX (ms) | Speed A100 TensorRT (ms) | Params (M) | FLOPs (G) |
|---|---|---|---|---|---|---|
| YOLOv9c | 640 | 53.0 | 239.1 | 2.05 | 25.3 | 102.1 |
| *px: pixels, ms: milliseconds, M: millions, B: billions* | | | | | | |

Table 1 summarizes the model features of YOLOv9c, presenting key metrics such as size in pixels (px), mean Average Precision on validation set (mAPval), speed in milliseconds (ms) for both CPU inference using ONNX and A100 TensorRT, parameters in millions (M), and Floating-Point Operations (FLOPs) in billions (G). YOLOv9c operates at a resolution of 640x640 pixels with a mAPval of 53.0. Its inference speed is 239.1 ms on CPU using ONNX and 2.05 ms on A100 TensorRT. With 25.3 million parameters and 102.1 billion FLOPs, YOLOv9c offers a balance between accuracy and computational efficiency for object detection tasks. Table 2 shows brief characteristics of YOLOv9c and compared to other models such as SSD MobileNet V1, SSD MobileNet V2, and Faster-RCNN ResNet-50 V1 which are previously present for stenosis detection [38].

Table 2
Brief characteristics of the models

| Model | Inference time, ms | mAP @[0.5:0.95] | Weights, M | Model size, Mb |
|---|---|---|---|---|
| YOLOv9c (Proposed Model) | 18 | 52.3 | 25.3 | 49 |
| SSD MobileNet V1 | 56 | 32 | 4.2 | 44 |
| SSD MobileNet V2 | 31 | 22 | 6.1 | 19 |
| SSD ResNet-50 V1 | 76 | 35 | 25.6 | 127 |
| Faster-RCNN ResNet-50 V1 | 89 | 30 | 25.6 | 114 |
| RFCN ResNet-101 V2 | 92 | 30 | 44.7 | 199 |
| Faster-RCNN ResNet-101 V2 | 106 | 32 | 44.7 | 190 |
| Faster-RCNN Inception ResNet V2 | 620 | 37 | 55.9 | 241 |
| Faster-RCNN NASNet | 540 | - | 88.9 | 416 |
| *ms: milliseconds, M: millions, Mb: megabytes* | | | | |

This table provides a concise overview of various object detection models' characteristics, focusing on inference time, mean Average Precision (mAP) in the range of IoU thresholds [0.5:0.95], weights in millions (M), and model size in megabytes (Mb). The proposed YOLOv9c model stands out with an inference time of 18 milliseconds and a competitive mAP of 52.3, weighing 25.3 million parameters with a model size of 49 Mb. Compared to other models such as SSD MobileNet V1, SSD MobileNet V2, and Faster-RCNN ResNet-50 V1, YOLOv9c offers superior performance in terms of both speed and accuracy, making it an efficient choice for real-time object detection applications.

In this study, the proposed YOLOv9c model is utilized as an object detection algorithm aimed at achieving high accuracy and real-time performance in detecting objects within images [42]. YOLOv9c represents a specific variant of the YOLO model that is tailored to meet the study's objectives [43]. Additionally, the study incorporates other well-established object detection models, such as SSD MobileNet V1, SSD MobileNet V2, SSD ResNet-50 V1, Faster-RCNN ResNet-50 V1, RFCN ResNet-101 V2, Faster-RCNN ResNet-101 V2, Faster-RCNN Inception ResNet V2, and Faster-RCNN NASNet, each of which offers distinct architectural features and performance characteristics [42, 44].

The utilization of SSD MobileNet V1, a lightweight convolutional neural network architecture, as the backbone of SSD reflects the study's consideration of computational efficiency without compromising accuracy in object detection tasks [45]. Furthermore, the upgraded version, SSD MobileNet V2, introduces new network building blocks and optimization techniques, enhancing the performance and efficiency of object detection [46]. Similarly, SSD ResNet-50 V1 and Faster-RCNN ResNet-50 V1 leverage the ResNet-50 architecture, known for its effectiveness in training deep models with numerous layers, to facilitate robust feature extraction and object detection [47, 48].

Moreover, the study incorporates Faster-RCNN ResNet-101 V2, which employs the deeper architecture of ResNet-101 V2 to enhance feature representations, potentially improving detection performance [49]. Additionally, the combination of the Faster-RCNN framework with the Inception-ResNet V2 architecture in Faster-RCNN Inception-ResNet V2 aims to leverage the exceptional accuracy and efficiency of Inception-ResNet V2 in image classification tasks for object detection purposes [50]. Furthermore, the integration of Faster-RCNN with the NASNet architecture in Faster-RCNN NASNet reflects the study's focus on optimizing network architecture using automatically designed neural networks [51].

These models were compared with the proposed model (YOLOv9c) in the present study, aiming to evaluate and compare their respective performances in object detection tasks. The detailed results are given in Table 3.

Table 3
Comparative study of the selected models.

| Model | Weights, M | | Training time, hours | | Inference time, ms | | F1-score | | mAP@0.5 | |
|---|---|---|---|---|---|---|---|---|---|---|
| | Abs. | Rel. | Abs. | Rel. | Abs. | Rel. | Abs. | Rel. | Abs. | Rel. |
| Proposed Model (YOLOv9c) | 25.3 | 6.1x | **11** | **0.6x** | **18** | **0.4x** | **0.98** | **1.36x** | **0.98** | **1.42x** |
| SSD MobileNet V1 | **4.2** | **1.0x** | 16 | 1.0x | 43 | 1.0x | 0.72 | 1.0x | 0.69 | 1.00x |
| SSD MobileNet V2 | 6.1 | 1.4x | 20 | 1.3x | 26 | 0.6x | 0.80 | 1.10x | 0.83 | 1.20x |
| SSD ResNet-50 V1 | 25.6 | 6.0x | 47 | 3.0x | 61 | 1.4x | 0.73 | 1.01x | 0.76 | 1.09x |
| Faster-RCNN ResNet-50 V1 | 25.6 | 6.0x | 28 | 1.8x | 98 | 2.3x | 0.88 | 1.21x | 0.92 | 1.33x |
| RFCN ResNet-101 V2 | 44.7 | 10.5x | 55 | 3.6x | 99 | 2.3x | 0.96 | 1.32x | 0.94 | 1.36x |
| Faster-RCNN ResNet-101 V2 | 44.7 | 10.5x | 55 | 3.5x | 118 | 2.7x | 0.96 | 1.32x | 0.94 | 1.35x |
| Faster-RCNN Inception ResNet V2 | 55.9 | 13.2x | 93 | 6.0x | 363 | 8.4x | 0.94 | 1.30x | 0.95 | 1.38x |
| Faster-RCNN NASNet | 88.9 | 21.0x | 147 | 9.5x | 880 | 20.4x | 0.82 | 1.13x | 0.84 | 1.22x |
| YOLOv8 | - | - | - | - | - | - | 0,68 | 0.94x | 0.65 | 0.94x |

*"Model": Names of different object detection models; "Weights (M)": Number of model weights in millions; "Training Time (hours)": Time taken to train the model in hours; "Inference Time (ms)": Time taken for inference or prediction per image in milliseconds; "F1-score"*:

*The F1-score is a metric used to assess the overall performance of a model by considering both precision and recall simultaneously.; "mAP@0.5": Mean Average Precision (mAP) at a threshold of 0.5 is a metric commonly used to evaluate object detection performance.*

Table 3 presents a comparative study of selected object detection models, including their absolute and relative weights in millions (M), training time in hours, inference time per image in milliseconds (ms), F1-score, and mean average precision at a threshold of 0.5 (mAP@0.5). The proposed YOLOv9c model

demonstrates superior performance in various aspects, including inference speed, F1-score, and mAP@0.5, compared to other models such as SSD MobileNet V1, SSD MobileNet V2, and Faster-RCNN ResNet-50 V1. Additionally, the table includes YOLOv8 for reference, highlighting the improvements achieved with YOLOv9c.

Table 4
Training parameters

| *Variable* | Values | *Variable* | Values | *Variable* | Values |
|---|---|---|---|---|---|
| *epochs* | 100 | *lrf* | 0.01 | *fl_gamma* | 0.0 |
| *batch_size* | 8 | *momentum* | 0.937 | *hsv_h* | 0.015 |
| *imgsz* | 640 | *weight_decay* | 0.0005 | *hsv_s* | 0.7 |
| *optimizer* | SGD | *warmup_epochs* | 3.0 | *hsv_v* | 0.4 |
| *workers* | 8 | *warmup_momentum* | 0.8 | *degrees* | 0.0 |
| *label_smoothing* | 0.0 | *warmup_bias_lr* | 0.1 | *translate* | 0.1 |
| *patience* | 100 | *box* | 7.5 | *scale* | 0.9 |
| *freeze* | [0] | *cls* | 0.5 | *shear* | 0.0 |
| *save_period* | -1 | *cls_pw* | 1.0 | *perspective* | 0.0 |
| *local_rank* | -1 | *obj* | 0.7 | *flipud* | 0.0 |
| *min_items* | 0 | *obj_pw* | 1.0 | *fliplr* | 0.5 |
| *close_mosaic* | 15 | *dfl* | 1.5 | *mosaic* | 1.0 |
| *bbox_interval* | -1 | *iou_t* | 0.2 | *mixup* | 0.15 |
| *lr0* | 0.01 | *anchor_t* | 5.0 | *copy_paste* | 0.3 |

Table 4 presents the training parameters used for the model, including values such as epochs, learning rate factor (lrf), focal loss gamma (fl_gamma), batch size, momentum, image size (imgsz), optimizer, and various augmentation parameters like hsv (hue, saturation, value), degrees, translation, scaling, shearing, perspective transformation, flipping, and mixup. These parameters are essential for configuring and fine-tuning the training process to achieve optimal performance for object detection tasks.

Table 4 provides a comparison of various object detection models based on several metrics. The models used include the proposed model (PM), SSD MobileNet V1 [38], SSD MobileNet V2 [38], SSD ResNet-50 V1 [38], Faster-RCNN ResNet-50 V1 [38], RFCN ResNet-101 V2 [38], Faster-RCNN ResNet-101 V2 [38], Faster-RCNN Inception ResNet V2 [38], Faster-RCNN NASNet [38] and YOLOv8 [52]. The metrics analyzed included the number of model weights (in millions), training time (in hours), inference time (in milliseconds), F1 score, and mAP@0.5 (Mean Average Precision at a threshold of 0.5).

Comparing the proposed model (PM) with the other models, we observe several noteworthy differences that highlight the advantages of the PM in terms of object detection performance.

In terms of model weights, the PM model yields a greater weight (25.3 million) than do the SSD MobileNet V1 (4.2 million) and SSD MobileNet V2 (6.1 million) models. This increase in weights suggests that the PM potentially incorporates more complex and expressive features, enabling it to capture finer details and improve detection accuracy.

Regarding training time, the PM demonstrated a training time 0.6 times shorter than that of the SSD MobileNet V1, indicating less resource consumption in the learning process.

The inference time, which reflects the speed of object detection during runtime, shows that the PM outperforms the SSD MobileNet V2, with an inference time of 18 milliseconds compared to 26 milliseconds. This improved inference efficiency suggests that the PM achieves real-time performance, making it suitable for time-sensitive applications.

Moving on to the evaluation metrics, the F1-score and mAP@0.5 provide insights into the detection accuracy of the models. The PM exhibited an F1-score of 0.98, surpassing the other models, including the SSD MobileNet V1 (0.72) and SSD MobileNet V2 (0.80). This higher F1-score implies that the PM achieves a better balance between precision and recall, resulting in more accurate object localization.

Similarly, the PM shows a superior mAP@0.5 of 0.98, outperforming the SSD MobileNet V1 (0.69) and SSD MobileNet V2 (0.83). A higher mAP@0.5 indicates that the PM excels at detecting objects with higher precision and recall rates at the specified threshold, making it well suited for applications demanding high detection performance.

Training was performed with the features explained in Table 4 by using 6660 images in the dataset (8325 total), and testing was performed with 832 images in the dataset. The trained images are labeled with red rectangles, as shown in Fig. 3. After training and testing were complete, validation was performed. Figure 4 shows the predicted stenosis and labels.

One hundred epochs were completed in 3.467 hours for fine-tuning. All of them were successfully completed. For validation, the YOLO 2024-3-18 Python-3.12.2, torch-2.2.1 + cu118, and CUDA:0 (NVIDIA RTX A4000, 16376MiB) was used, and the model summary is given in Table 5.

Table 5
Summary of the validation model

| Class | Images | Instances | Box | | | |
|---|---|---|---|---|---|---|
| | | | P | R | mAP@50 | mAP@50–95 |
| All | 832 | 832 | 0.969 | 0.965 | 0.978 | 0.518 |

Table 5 summarizes the validation results of the model, including metrics such as precision (P), recall (R), mean Average Precision at IoU threshold 0.5 (mAP@50), and mean Average Precision over the range of IoU thresholds from 0.5 to 0.95 (mAP@50–95). The evaluation is performed across all classes, comprising a total of 832 images and instances. The model demonstrates strong performance, with high precision, recall, and mAP scores, indicating its effectiveness in object detection tasks.

As shown in Fig. 5, the speed results for validation for preprocessing, inference, loss, and postprocessing were 0.2 ms, 3.9 ms, 0.0 ms, and 1.3 ms per image, respectively.

The confusion matrix illustrated in Fig. 6 reveals interesting insights into the object detection performance, specifically for the class "stenosis" and the background class. The number of instances classified as "stenosis" is 820, while the background class consists of 10 instances. However, it is worth noting that the model predicted 12 instances as background instead of correctly identifying them as "stenosis".

This observation highlights an important aspect of the object detection system's performance. The misclassification of 12 instances as background indicates a potential limitation in the model's ability to accurately differentiate between the "Stenosis" class and the background. This misclassification can have implications in medical imaging or other applications where correctly identifying "stenosis" is crucial.

# 4. Discussion

The development of a novel stenosis detection algorithm for patients with multivessel CAD represents a significant advancement in addressing the challenges associated with accurate diagnosis and interpretation in this complex patient population. The automation of multivessel CAD detection and grading has the potential to streamline the workflow of operators, minimize the risk of misinterpretation, and expedite treatment decision-making, ultimately improving patient care and outcomes.

Traditionally, the interpretation of coronary angiograms relies heavily on the expertise of operators to identify stenosis locations and describe various aspects of the coronary vasculature, necessitating a comprehensive understanding of vessel characteristics and stenotic segment details. In this study, the algorithm was initially tested for detecting single-vessel CAD, serving as an initial evaluation of its capabilities for the primary task of multivessel CAD detection. The successful application of the YOLOv9c model in achieving remarkable performance in terms of processing speed and detection accuracy underscores its potential for real-time detection of coronary artery stenosis and severity grading, which is essential for accurate CAD diagnosis and treatment.

The ability to perform real-time detection and simultaneous grading of stenotic lesions in the cath-lab significantly improves diagnostic efficiency, suggesting the potential to guide treatment decisions without the need for additional contrast agent injections, particularly in cases where rapid interventions, such as myocardial infarction, are crucial. By reducing the time required for accurate diagnosis, the

algorithm can streamline the decision-making process, leading to faster interventions and improved patient outcomes, particularly in critical cases.

The integration of advanced algorithms, such as YOLOv9c, in the context of multivessel CAD detection and grading represents a significant step toward enhancing the diagnostic capabilities and efficiency of cardiovascular imaging technologies. The potential of these advancements to improve patient care and outcomes underscores the importance of continued research and development in the field of medical imaging and diagnostic algorithms.

# 5. Conclusion

In conclusion, our study successfully developed a novel stenosis detection algorithm utilizing the YOLOv9c model, which demonstrated exceptional performance in terms of processing speed and detection accuracy, meeting essential criteria for efficient CAD diagnosis and treatment. The automation of multivessel CAD detection and grading has the potential to significantly improve diagnostic efficiency, minimize the risk of misinterpretation, and expedite treatment decision-making, ultimately benefiting patients with multivessel CAD. Future research should focus on further validation, incorporate larger datasets, and address potential limitations to ensure the practical implementation of the algorithm in clinical settings.

The successful development of the stenosis detection algorithm using the YOLOv9c model represents a significant advancement in the field of cardiovascular imaging and diagnostic algorithms. The exceptional performance of the algorithm in terms of processing speed and detection accuracy underscores its potential to revolutionize the diagnostic process, ultimately leading to improved patient care and outcomes. The integration of advanced algorithms in cardiovascular imaging represents a critical aspect of optimizing diagnostic efficiency and accuracy, emphasizing the need for ongoing advancements in medical imaging research and technology.

Furthermore, the potential of the algorithm to streamline the decision-making process and expedite interventions, particularly in critical cases such as myocardial infarction, highlights its significant clinical implications. By reducing the time required for accurate diagnosis, the algorithm can lead to faster interventions and improved patient outcomes, particularly in severe cases. The successful implementation of the algorithm in clinical settings has the potential to significantly impact patient care and outcomes, emphasizing the importance of continued research and development in the field of medical imaging and diagnostic algorithms.

In summary, the development of a stenosis detection algorithm using the YOLOv9c model represents a critical advancement in addressing the challenges associated with multivessel CAD detection and grading. The potential of the algorithm to improve diagnostic efficiency, minimize the risk of misinterpretation, and expedite treatment decision-making underscores its significance in the field of cardiovascular imaging and patient care. The successful implementation of the algorithm in clinical

settings has the potential to significantly impact patient outcomes, emphasizing the importance of ongoing advancements in medical imaging research and technology.

# Declarations

**Author contributions** H.İ.K. and M.A. wrote the main manuscript text. M.A., and H.A.A. prepared the models and results, M.A., H.İ.K., and H.A.A. were responsible for reviewing and editing the manuscript. H.A.A. and Ş.T were responsible for supervising the research. All authors reviewed the manuscript.

**Funding** The authors declare that no funds, grants, or other support were received during this study.

**Data Availability** The publicly accessible “Angiographic dataset for stenosis detection” database is utilized in this work [39].

**Ethical approval** This article does not contain any studies with human participants performed by any of the authors.

**Conflict of interest** The authors declare that they have no known competing financial interests or personal relationships that could have appeared to influence the work reported in this paper.

**Competing interests** The authors declare that they have no conflict of interest.

# References

1. S. Cacciatore *et al.*, "Management of Coronary Artery Disease in Older Adults: Recent Advances and Gaps in Evidence," *J Clin Med,* vol. 12, no. 16, p. 5233, Aug 11 2023, doi: https://doi.org/10.3390/jcm12165233.
2. W. Lieb *et al.*, "Genetic predisposition to higher blood pressure increases coronary artery disease risk," *Hypertension,* vol. 61, no. 5, pp. 995-1001, May 2013, doi: https://doi.org/10.1161/HYPERTENSIONAHA.111.00275.
3. C. Tcheandjieu *et al.*, "Large-scale genome-wide association study of coronary artery disease in genetically diverse populations," *Nat Med,* vol. 28, no. 8, pp. 1679-1692, Aug 2022, doi: https://doi.org/10.1038/s41591-022-01891-3.
4. J. van Setten *et al.*, "Genome-wide association study of coronary and aortic calcification implicates risk loci for coronary artery disease and myocardial infarction," *Atherosclerosis,* vol. 228, no. 2, pp. 400-5, Jun 2013, doi: https://doi.org/10.1016/j.atherosclerosis.2013.02.039.
5. K. Red-Horse *et al.*, "Coronary arteries form by developmental reprogramming of venous cells," *Nature 2010 464:7288,* vol. 464, no. 7288, 2010, doi: https://doi.org/10.1038/nature08873.
6. F. Dong, W. M. Chilian, and L. Yin, "Knowns and unknowns of coronary artery development and anomalies," *International journal of cardiology,* vol. 281, 2019, doi: https://doi.org/10.1016/j.ijcard.2019.01.073.

7. Y. Tang, Y. Zhang, Y. Chen, Y. Xiang, and Y. Xie, "Role of the microRNA, miR-206, and its target PIK3C2α in endothelial progenitor cell function – potential link with coronary artery disease," *The FEBS Journal,* vol. 282, no. 19, 2015, doi: https://doi.org/10.1111/febs.13372.
8. F. E. Anaibar *et al.*, "Analysis of the genetic predisposition to develop a Myocardial Infarction in a sample of Moroccan patients," *E3S Web of Conferences,* vol. 319, no. International Congress on Health Vigilance (VIGISAN 2021), 2021, doi: https://doi.org/10.1051/e3sconf/202131901013.
9. H. Basit, A. Kahn, S. Zaidi, H. Chadow, and A. Khan, "A Case of ST-Elevation Myocardial Infarction With Right Bundle Branch Block, an Ominous Sign of Critical Coronary Occlusion," *Cureus,* 2022, doi: https://doi.org/10.7759/cureus.21216.
10. I. Kormi *et al.*, "Matrix metalloproteinase-8 and tissue inhibitor of matrix metalloproteinase-1 predict incident cardiovascular disease events and all-cause mortality in a population-based cohort," *European Journal of Preventive Cardiology,* vol. 24, no. 11, 2017, doi: https://doi.org/10.1177/2047487317706585.
11. M. D. Waltmann, J. E. Basford, E. S. Konaniah, N. L. Weintraub, and D. Y. Hui, "Apolipoprotein E receptor-2 deficiency enhances macrophage susceptibility to lipid accumulation and cell death to augment atherosclerotic plaque progression and necrosis," *Biochimica et Biophysica Acta (BBA) - Molecular Basis of Disease,* vol. 1842, no. 9, pp. 1395-405, Sep 2014, doi: https://doi.org/10.1016/j.bbadis.2014.05.009.
12. R. A. Nataraj, S. Shivaprasad, V. K. Methuku, and S. B. Raja, "Study of prevalence of asymptomatic coronary artery disease in patients with diabetes mellitus by treadmill test," *International Journal of Advanced Research in Medicine,* vol. 3, no. 1, pp. 158-162, 2021, doi: https://doi.org/10.22271/27069567.2021.v3.i1c.121.
13. T. Chadashvili, D. Litmanovich, F. Hall, and P. J. Slanetz, "Do breast arterial calcifications on mammography predict elevated risk of coronary artery disease?," *European Journal of Radiology,* vol. 85, no. 6, pp. 1121-4, Jun 2016, doi: https://doi.org/10.1016/j.ejrad.2016.03.006.
14. A. M. Sobhy, A. M. F. Eldeek, and E. M. A. El-Hamid, "The Role of Breast Arterial Calcification on Mammogram as a Predictor for Risk of Coronary Artery Disease in Women," *The Scientific Journal of Medical Scholar,* vol. 1, no. 3, 2022, doi: https://doi.org/10.55675/sjms.v1i3.18.
15. T. Thom, "American Heart Association Statistics Committee and Stroke Statistics Subcommittee : Heart disease and stroke statistical-2006 update : A report from the American Heart Association Statistics Committee and Stroke statistics subcommittee," *Circulation,* vol. 113, pp. e85-e151, 2006 2006. [Online]. Available: https://cir.nii.ac.jp/crid/1574231875404477440.
16. R. Bonita and R. Beaglehole, "Trends in cerebrovascular disease mortality in New Zealand," (in eng), *N Z Med J,* vol. 95, no. 710, pp. 411-414, 1982/06// 1982. [Online]. Available: http://europepmc.org/abstract/MED/6955662.
17. E. D. Hoffman, Jr., B. S. Klees, and C. A. Curtis, "Overview of the Medicare and Medicaid Programs," (in eng), *Health Care Financ Rev,* vol. 22, no. 1, pp. 175-193, Fall 2000.

18. C. W. Tsao *et al.*, "Heart Disease and Stroke Statistics—2023 Update: A Report From the American Heart Association," *Circulation,* vol. 147, no. 8, 2023, doi: https://doi.org/10.1161/CIR.0000000000001123.
19. N. C. f. H. Statistics, "Multiple Cause of Death 2018–2021 on CDC WONDER Database," *Accessed February,* vol. 2, 2023.
20. G. A. Roth *et al.*, "Global, regional, and national burden of cardiovascular diseases for 10 causes, 1990 to 2015," *Journal of the American college of cardiology,* vol. 70, no. 1, pp. 1-25, Jul 4 2017, doi: https://doi.org/10.1016/j.jacc.2017.04.052.
21. R. Ferrari *et al.*, "Geographical variations in the prevalence and management of cardiovascular risk factors in outpatients with CAD: Data from the contemporary CLARIFY registry," *European Journal of Preventive Cardiology,* vol. 22, no. 8, 2015, doi: https://doi.org/10.1177/2047487314547652.
22. R. Lozano *et al.*, "Global and regional mortality from 235 causes of death for 20 age groups in 1990 and 2010: a systematic analysis for the Global Burden of Disease Study 2010," *The Lancet,* vol. 380, no. 9859, 2012, doi: https://doi.org/10.1016/S0140-6736(12)61728-0.
23. M. Correction Naghavi *et al.*, "Global, regional, and national age-sex specific all-cause and cause-specific mortality for 240 causes of death, 1990-2013: A systematic analysis for the Global Burden of Disease Study 2013," *THE LANCET,* vol. 385, no. 9963, 2015, doi: https://doi.org/10.1016/S0140-6736(14)61682-2.
24. C. Martin-Isla *et al.*, "Image-Based Cardiac Diagnosis With Machine Learning: A Review," *Frontiers in Cardiovascular Medicine,* vol. 7, 2020, doi: https://doi.org/10.3389/fcvm.2020.00001.
25. L. Yi *et al.*, "Detection of Self-explosive Insulators in Aerial Images Based on Improved YOLO v4," *Journal of Physics: Conference Series,* vol. 2320, no. 1, 2022, doi: https://doi.org/10.1088/1742-6596/2320/1/012025.
26. C.-Y. Wang, A. Bochkovskiy, and H.-Y. M. Liao, "YOLOv7: Trainable bag-of-freebies sets new state-of-the-art for real-time object detectors," in *Proceedings of the IEEE/CVF conference on computer vision and pattern recognition*, 2023, pp. 7464-7475, doi: https://doi.org/10.1109/CVPR52729.2023.00721.
27. K. Liu, "STBi-YOLO: A Real-Time Object Detection Method for Lung Nodule Recognition | IEEE Journals & Magazine | IEEE Xplore," *IEEE Access,* vol. 10, pp. 75385-75394, 2022, doi: https://doi.org/10.1109/ACCESS.2022.3192034.
28. S. N. Chotimah, B. Warsito, and B. Surarso, "Chronic Kidney Disease Diagnosis System using Sequential Backward Feature Selection and Artificial Neural Network," *E3S Web of Conferences,* vol. 317, no. The 6th International Conference on Energy, Environment, Epidemiology, and Information System (ICENIS 2021), 2021, doi: https://doi.org/10.1051/e3sconf/202131705030.
29. H. Liu, A. L. Bamba, Y. Gan, H. Liu, A. L. Bamba, and Y. Gan, "Uncertainty measurement and confidence calibration for calcium detection in optical coherence images," *Proceedings Volume 12367, Optical Coherence Tomography and Coherence Domain Optical Methods in Biomedicine XXVII,* vol. 12367, 2023, doi: https://doi.org/10.1117/12.2652944.

30. H. Lee *et al.*, "Identification of Acute Giant Cell Arteritis in Real-World Data Using Administrative Claims-Based Algorithms," *ACR Open Rheumatology,* vol. 3, no. 2, 2021, doi: https://doi.org/10.1002/acr2.11218.
31. Q. Li, B. Guo, H. Jin, D. Guo, Z. Ma, and C. Kang, "Application of Object Detection Algorithm Based on Deep Learning in Classification of Wild Ginseng Grades | IEEE Conference Publication | IEEE Xplore," *2023 2nd International Conference on Artificial Intelligence, Human-Computer Interaction and Robotics (AIHCIR),* 2023, doi: https://doi.org/10.1109/AIHCIR61661.2023.00024.
32. Y. Li *et al.*, "A Preprocessing Method for Coronary Artery Stenosis Detection Based on Deep Learning," *Algorithms 2024, Vol. 17, Page 119,* vol. 17, no. 3, 2024, doi: https://doi.org/10.3390/a17030119.
33. X. Hu *et al.*, "Researches advanced in application of medical image analysis based on deep learning," in *Proceedings Volume 12288, International Conference on Computer, Artificial Intelligence, and Control Engineering (CAICE 2022)*, 2022, vol. 12288, doi: https://doi.org/10.1117/12.2641098. [Online]. Available: https://www.spiedigitallibrary.org/conference-proceedings-of-spie/12288/1228812/Researches-advanced-in-application-of-medical-image-analysis-based-on/10.1117/12.2641098.short
34. K. Grishin, S. Mei, and S. Ilić, "YOLO–CL: Galaxy cluster detection in the SDSS with deep machine learning," *Astronomy & Astrophysics,* vol. 677, 2023, doi: https://doi.org/10.1051/0004-6361/202345976.
35. M. Saatchi *et al.*, "Accuracies of genomic breeding values in American Angus beef cattle using K-means clustering for cross-validation," *Genetics Selection Evolution 2011 43:1,* vol. 43, no. 1, p. 40, Nov 28 2011, doi: https://doi.org/10.1186/1297-9686-43-40.
36. X. Pan *et al.*, "A Comprehensive Review of Natural Products against Liver Fibrosis: Flavonoids, Quinones, Lignans, Phenols, and Acids," *Evidence-Based Complementary and Alternative Medicine,* vol. 2020, p. 7171498, 2020, doi: https://doi.org/10.1155/2020/7171498.
37. C.-Y. Wang, I.-H. Yeh, and H.-Y. M. Liao, "YOLOv9: Learning What You Want to Learn Using Programmable Gradient Information," *arXiv preprint arXiv:2402.13616,* 2024, doi: https://doi.org/10.48550/arXiv.2402.13616.
38. V. V. Danilov *et al.*, "Real-time coronary artery stenosis detection based on modern neural networks," *Scientific Reports 2021 11:1,* vol. 11, no. 1, p. 7582, Apr 7 2021, doi: https://doi.org/10.1038/s41598-021-87174-2.
39. V. K. Danilov, Kirill; Kutikhin, Anton; Gerget, Olga; Frangi, Alejandro; Ovcharenko, Evgeny. *Angiographic dataset for stenosis detection*, Mendeley Data, doi: https://doi.org/10.17632/ydrm75xywg.1.
40. J. Redmon, S. Divvala, R. Girshick, and A. Farhadi, "You only look once: Unified, real-time object detection," in *Proceedings of the IEEE conference on computer vision and pattern recognition*, 2016, pp. 779-788, doi: https://doi.org/10.1109/CVPR.2016.91.
41. J. Redmon and A. Farhadi, "YOLO9000: better, faster, stronger," in *Proceedings of the IEEE conference on computer vision and pattern recognition*, 2017, pp. 7263-7271, doi:

https://doi.org/10.1109/cvpr.2017.690.

42. R. Girshick, J. Donahue, T. Darrell, and J. Malik, "Rich feature hierarchies for accurate object detection and semantic segmentation," in *Proceedings of the IEEE conference on computer vision and pattern recognition*, 2014, pp. 580-587, doi: https://doi.org/10.1109/CVPR.2014.81.
43. R. Su, W. Huang, H. Ma, X. Song, and J. Hu, "SGE NET: Video Object Detection with Squeezed GRU and Information Entropy Map | IEEE Conference Publication | IEEE Xplore," *2021 IEEE International Conference on Image Processing (ICIP),* 2021, doi: https://doi.org/10.1109/ICIP42928.2021.9506081.
44. S. S, "Significance of Screening the General Population for Potential Cardiovascular Diseases with a Combination Assay of B-type Natriuretic Peptide and High Sensitive Troponin I," *Journal of Medical Diagnostic Methods,* vol. 06, no. 02, p. 2, 2017, doi: https://doi.org/10.4172/2168-9784.1000240.
45. Q. B. Phan and T. T. Nguyen, "A Novel Approach for PV Cell Fault Detection Using YOLOv8 and Particle Swarm Optimization," in *2023 IEEE 66th International Midwest Symposium on Circuits and Systems (MWSCAS)*, 6-9 Aug. 2023 2023, pp. 634-638, doi: https://doi.org/10.1109/MWSCAS57524.2023.10406139.
46. P. Ruiz-Ponce *et al.*, "POSEIDON: A Data Augmentation Tool for Small Object Detection Datasets in Maritime Environments," *Sensors 2023, Vol. 23, Page 3691,* vol. 23, no. 7, 2023, doi: https://doi.org/10.3390/s23073691.
47. I. S. Mohamed and L. K. Chuan, "PAE: Portable Appearance Extension for Multiple Object Detection and Tracking in Traffic Scenes | IEEE Journals & Magazine | IEEE Xplore," *IEEE Access,* vol. 10, pp. 37257-37268, 2022, doi: https://doi.org/10.1109/ACCESS.2022.3160424.
48. H. Lou *et al.*, "DC-YOLOv8: Small-Size Object Detection Algorithm Based on Camera Sensor," *Electronics 2023, Vol. 12, Page 2323,* vol. 12, no. 10, 2023, doi: https://doi.org/10.3390/electronics12102323.
49. K. He, G. Gkioxari, P. Dollár, and R. Girshick, "Mask r-cnn," in *Proceedings of the IEEE international conference on computer vision*, 2017, pp. 2961-2969, doi: https://doi.org/10.1109/ICCV.2017.322.
50. H. Liu *et al.*, "SF-YOLOv5: A Lightweight Small Object Detection Algorithm Based on Improved Feature Fusion Mode," *Sensors 2022, Vol. 22, Page 5817,* vol. 22, no. 15, 2022, doi: https://doi.org/10.3390/s22155817.
51. D. Guarin, J. Wong, and A. Ramirez-Zamora. (2023). An Artificial Intelligence Video-Based Assessment of Upper-limb Bradykinesia in Parkinson's Disease. Available: https://www.researchsquare.com/article/rs-3092935/latest
52. M. Osama, R. Kumar, and M. Shahid, "Empowering Cardiologists with Deep Learning YOLOv8 Model for Accurate Coronary Artery Stenosis Detection in Angiography Images," in *2023 International Conference on IoT, Communication and Automation Technology (ICICAT)*, 2023: IEEE, pp. 1-6, doi: https://doi.org/10.1109/ICICAT57735.2023.10263760.

# Figures

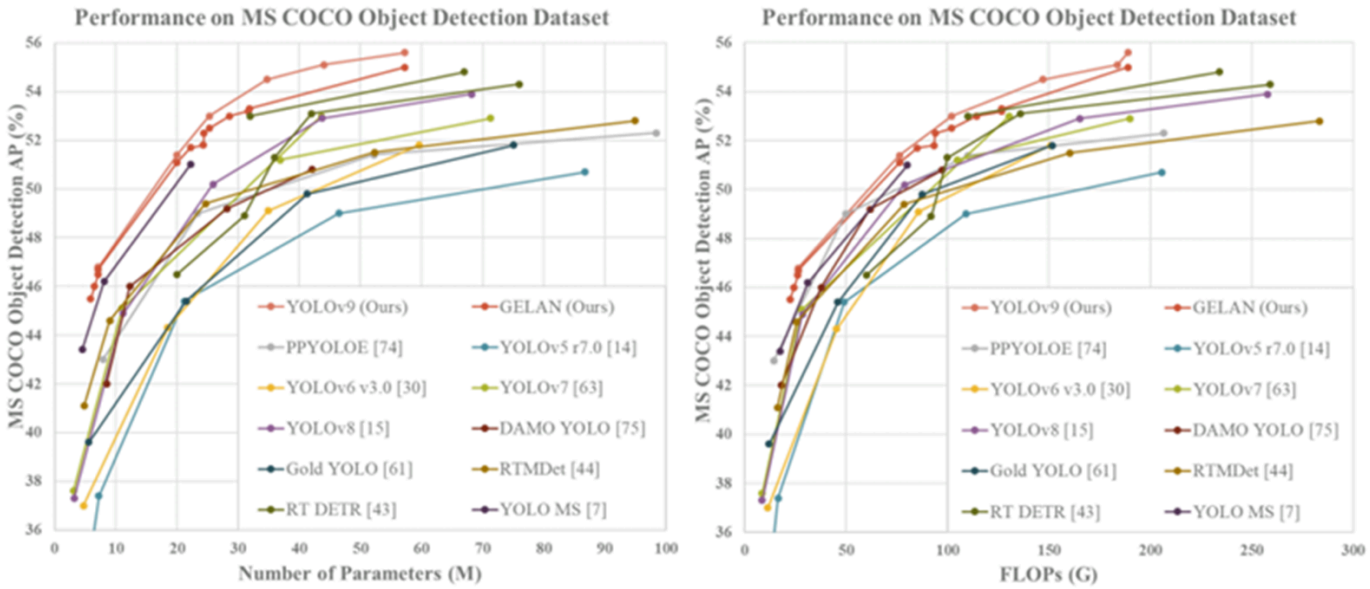


## Figure 1

*YOLOv9 versus state-of-the-art real-time object detectors [37].*

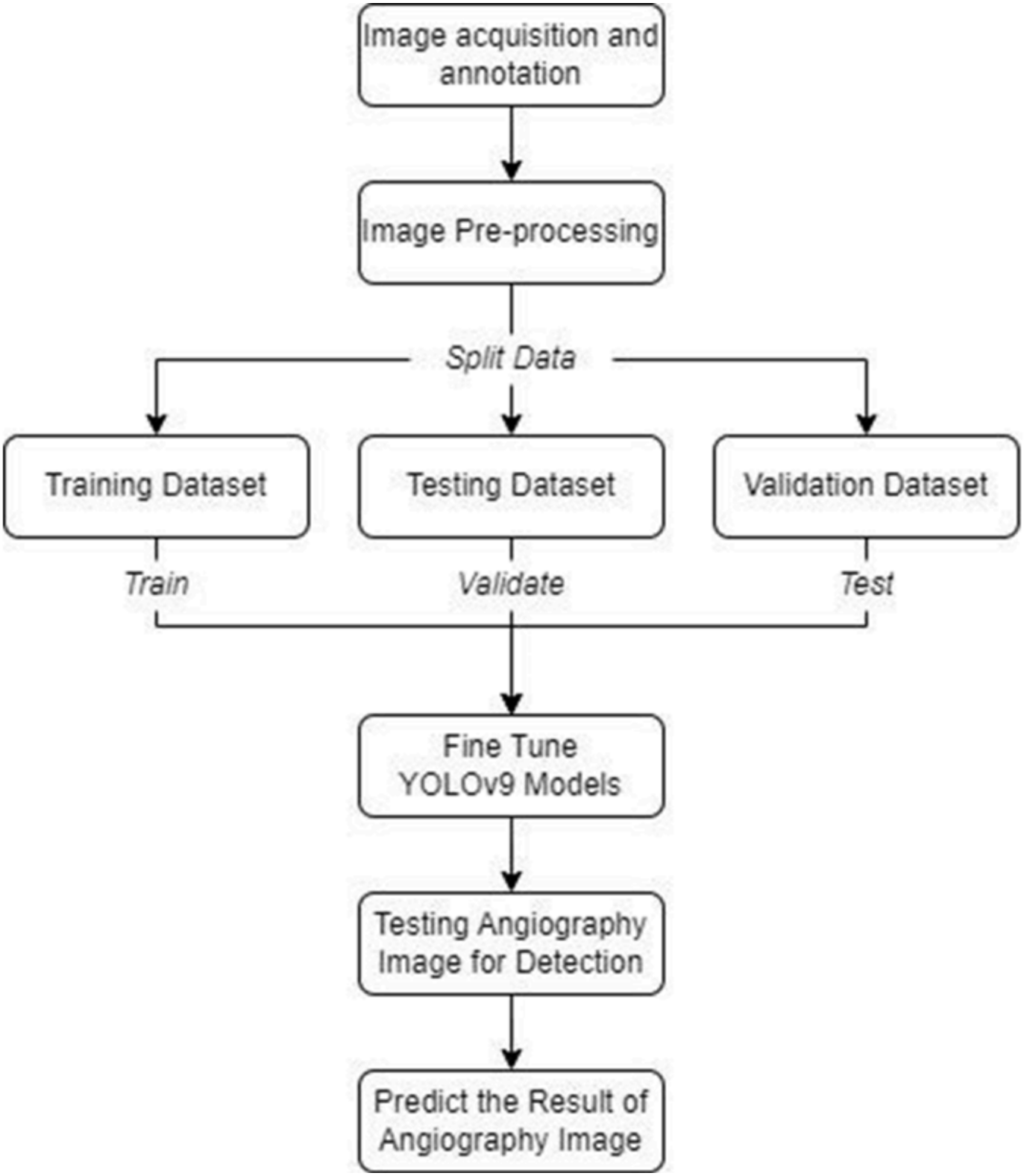


**Figure 2**

*Flowchart of proposed framework*

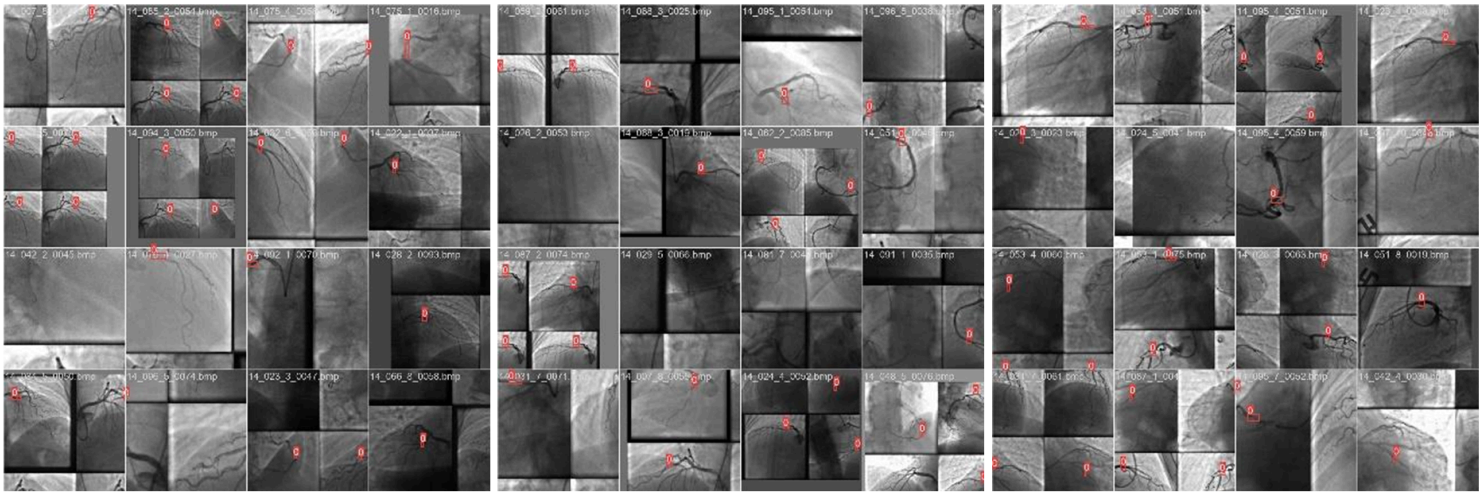

a) b) c)

## Figure 3

*Training batch boxes from 6660 images are illustrated in a, b, and c. Red marked rectangles show the labeled stenosis*

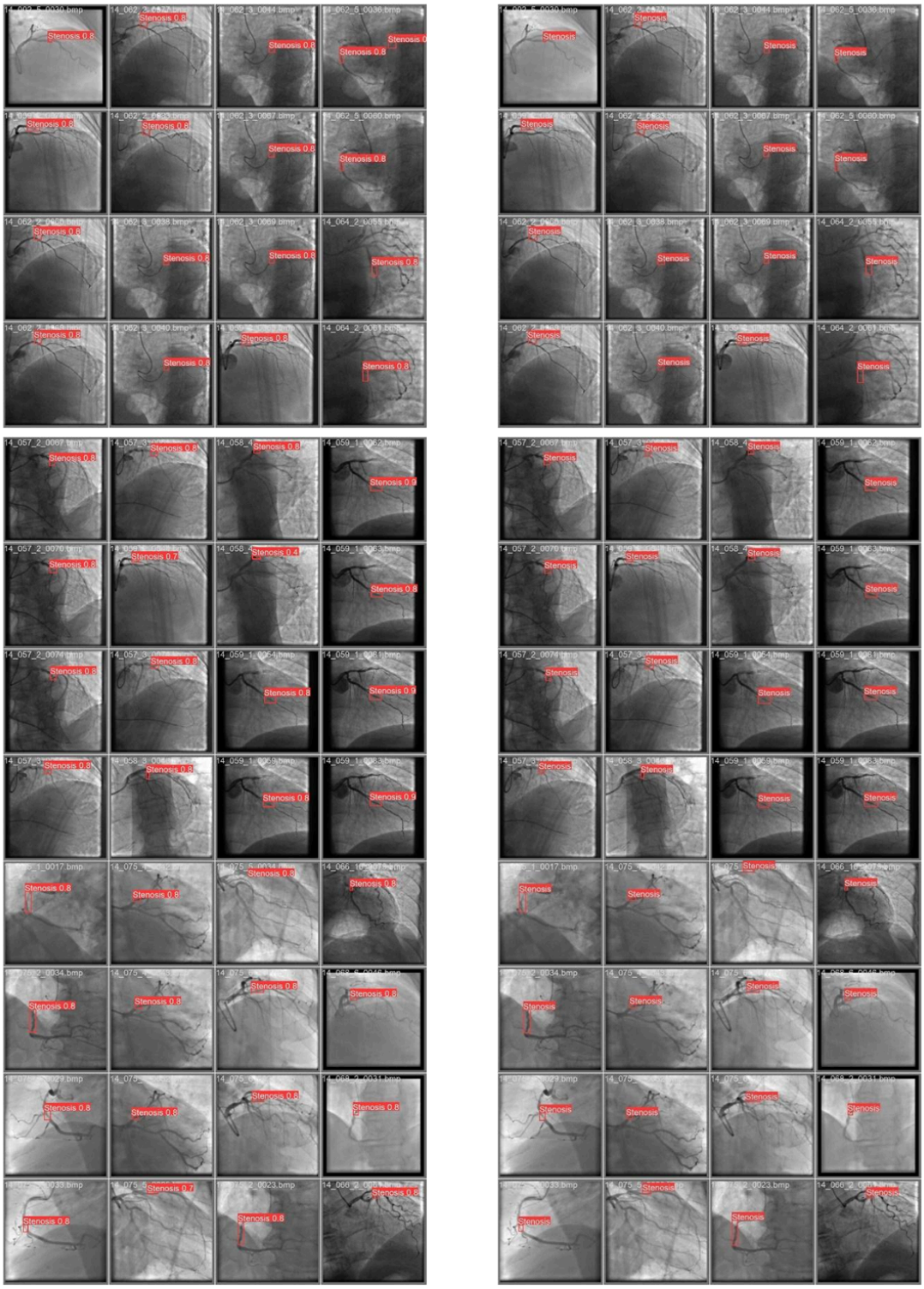


## Figure 4

*a) The predicted stenosis is marked with a red rectangle and written as stenosis on boxes. b) The labeled images of the original stenosis (marked as a red rectangle).*

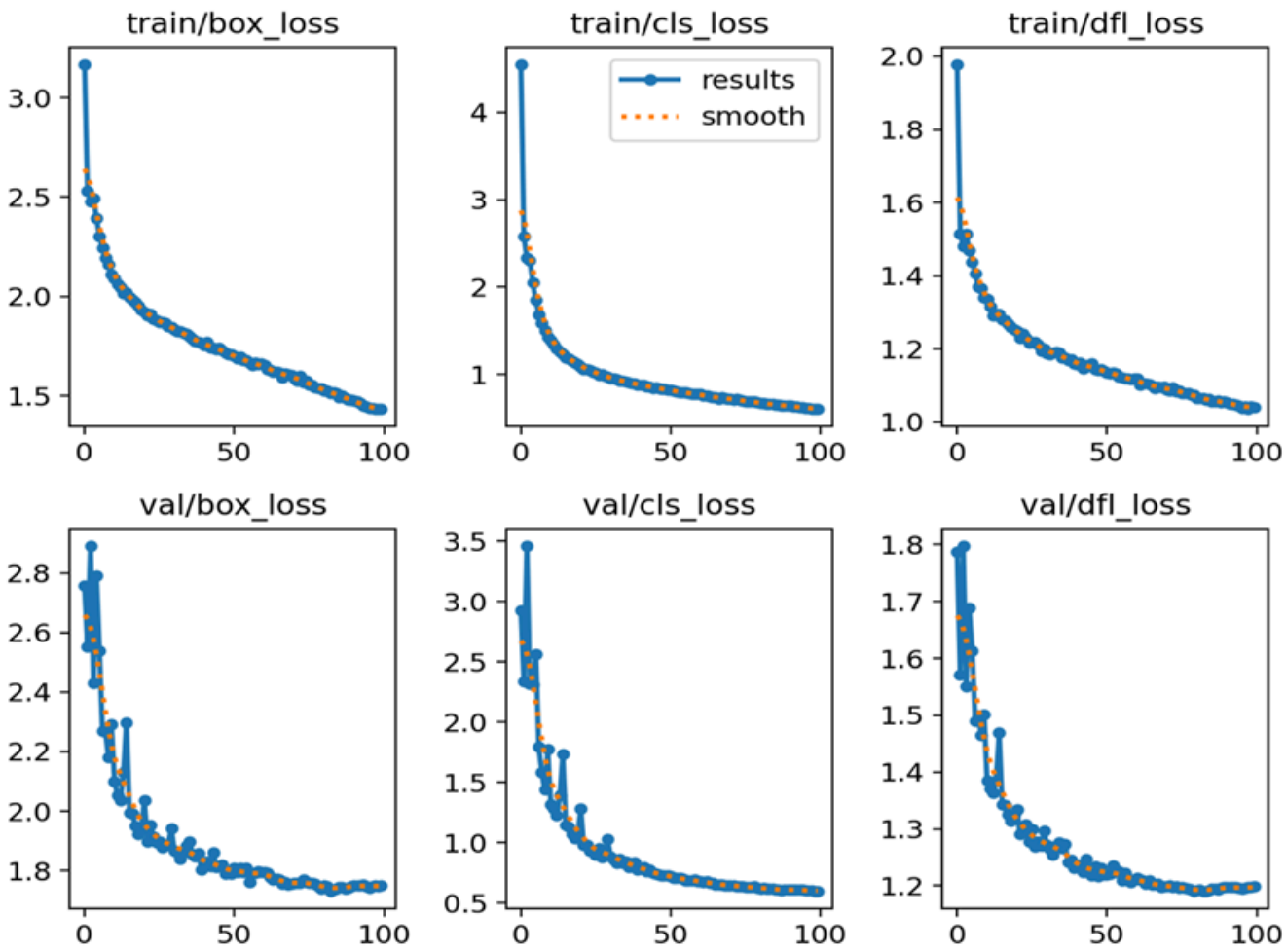


**Figure 5**

*Train and validation results for box box_loss, cls_loss and dfl_loss*

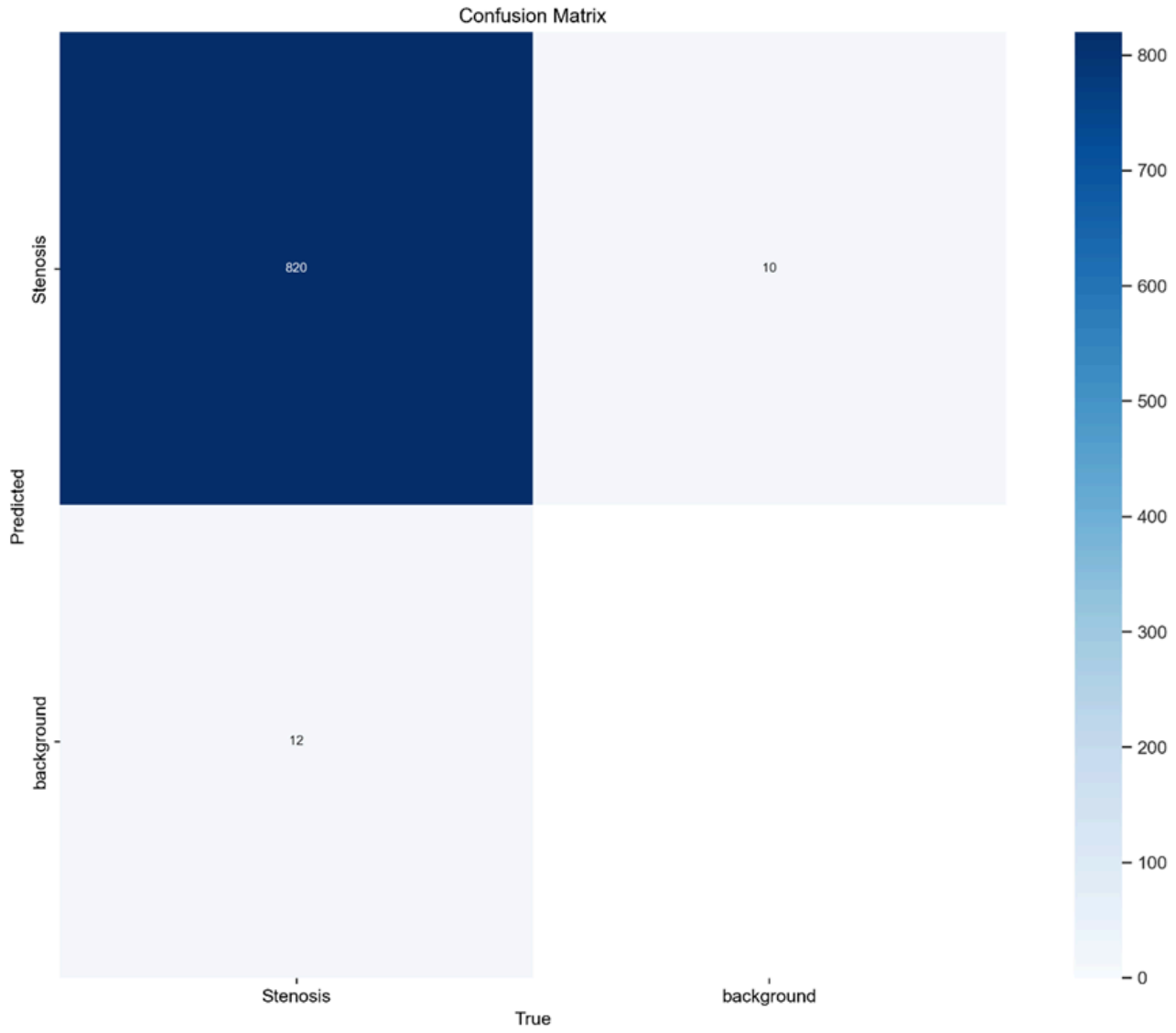


## Figure 6

*The stenosis, predicted and background confusion matrix*